Applied Physics Express

Simultaneous excitation of two different spinwave modes by optical ultrafast demagnetization

To cite this article: Sang-Jun Yun *et al* 2015 *Appl. Phys. Express* **8** 063009

Applied Physics Express **8**, 063009 (2015)
http://dx.doi.org/**10.7567/APEX.8.063009**

Simultaneous excitation of two different spinwave modes by optical ultrafast demagnetization

Sang-Jun Yun, Cheong-Gu Cho, and Sug-Bong Choe*

Department of Physics and Institute of Applied Physics, Seoul National University, Seoul 151-747, Republic of Korea
E-mail: sugbong@snu.ac.kr

Received March 4, 2015; accepted May 3, 2015; published online May 28, 2015

We report here an experimental technique to generate spinwaves using femtosecond laser pulses. The femtosecond laser pulses induce ultrafast demagnetization, which causes the propagation of the spinwaves from the laser spot. The observed spinwaves exhibit an anisotropic behavior by showing both the forward and backward modes depending on the propagation direction with respect to the in-plane magnetization direction, as confirmed by micromagnetic simulations. The forward mode is found to propagate over a few micrometers with small dissipation, providing a possible spinwave source.

Spinwaves are ordering states of the magnetization excited from an equilibrium state. The spinwaves in thin metallic magnetic films have attracted considerable attention recently in studies on magnetic recording and spintronics devices.[1–4] Such spinwaves have long been studied by ferromagnetic resonance and Brillouin light scattering techniques in the frequency domain to analyze the magnonic characteristics.[5–9] Recently, it has become possible to directly observe the spinwaves in the time domain by real-time optical and electric measurement techniques.[10–16] Such spinwaves have been generated by either thermal[5] or electric excitation.[9–14] It has recently been reported that an optical excitation can also generate the spinwaves via either the inverse Faraday effect[15] or the ultrafast demagnetization.[16] In this study, we report an experimental observation that the ultrafast demagnetization technique can generate two different spinwave modes — backward volume and forward surface modes — depending on the propagation direction.

For this study, an optical setup of the two-color pump–probe measurement was developed, as shown in Fig. 1(a). In this setup, 100 fs Ti:sapphire laser pulses with 94 MHz repetition rate and 800 nm wavelength were used as the pump beams to excite the spinwaves. The second-harmonic laser pulses of 400 nm wavelength were then used as the probe beams to observe the spinwave propagation behaviors. By using an objective lens with a high numerical aperture (0.9), the probe beam was focused onto the sample with the diffraction limit down to about 350 nm, as measured by the knife edge method.[17] At the present alignment, the diameter of the pump beam was measured to be about 800 nm. The time delay t between the pump and probe beams was adjusted using an optical delay line. By tilting the half mirror (HM) in the setup, the position of the probe beam spot can be scanned around the pump beam spot as illustrated in Fig. 1(b), and thus one can construct two-dimensional magnetization images. The distance between the pump and probe beam spots was estimated by measuring the lateral shift between the images captured using either the pump or probe beam. The magnetic signal was obtained using the polar magneto-optical Kerr effect (p-MOKE). In order to enhance the signal-to-noise ratio of the measurements, the probe beam was modulated by a photoelastic modulator (PEM) at 50 kHz and detected by a balanced detector connected to lock-in amplifiers. The detected signal was then normalized by the DC signal to eliminate fluctuations in light intensities and possible thermal artifact.

The present optical setup was applied to a 30-nm-thick ferromagnetic $Co_{40}Fe_{40}B_{20}$ thin film with in-plane magnetic anisotropy, sputtered on a Si substrate with a 300-nm-thick SiO_2 layer. The coercive and anisotropic fields of the film were determined to be 1.5 ± 0.5 mT and 1.5 ± 0.2 T, respectively, from a VSM measurement. In this experiment, an in-plane magnetic field H_x was applied along the x-axis. Since the strength of H_x (= 90 mT) was sufficiently larger than the coercive field, the initial magnetization direction was aligned to the x-axis. To induce a coherent spinwave excitation, an

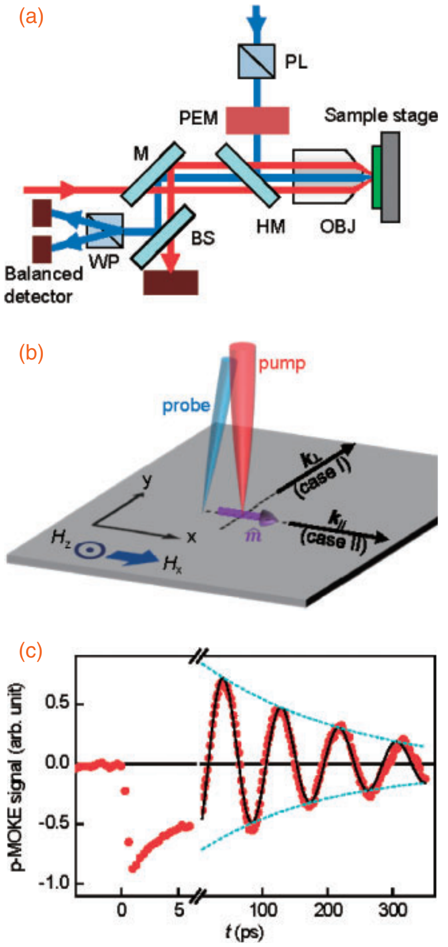

Fig. 1. (a) Schematic diagram of the measurement system with a polarizer (PL), a half mirror (HM), an objective lens (OBJ), a mirror (M), a beam splitter (BS), and a Wollaston prism (WP). The red and blue lines show the pump and probe beam paths, respectively. (b) Experimental geometries of Cases I and II. The probe beam spot is scanned around the pump beam spot. The black arrow labeled $k_\perp$ ($k_\parallel$) indicates the wavevector $\vec{k}$ perpendicular (parallel) to the magnetization $\hat{m}$. (c) Temporal variation of the p-MOKE signal measured at the pump beam center. The black solid line shows the best fit with a damped harmonic oscillation, and the cyan solid lines guide the amplitude decay.

out-of-plane magnetic field H_z ($= 390\,\mathrm{mT}$) was simultaneously applied to the film to tilt the magnetization slightly toward the $+z$-axis. The tilting angle of the magnetization was estimated to be about 14° from the sample plane. The pump-beam excitation then induced the ultrafast demagnetization within a few picoseconds, followed by a damped precession over a few hundred picoseconds, as shown in Fig. 1(c). The precession angular frequency ω_p at the center was determined to be $(70.7 \pm 0.6) \times 10^9\,\mathrm{rad/s}$ by fitting with a damped harmonic oscillation, as shown by the black solid line of the best fit. This precession at the center acted as a spinwave source and consequently emitted the spinwaves outward. Two spinwave modes were then examined depending on the propagation geometry as shown in Fig. 1(b): either the spinwave vector $\vec{k}$ is perpendicular to the magnetization direction $\hat{m}$ (Case I) or $\vec{k}$ is parallel to $\hat{m}$ (Case II). The fluence of the pump pulses was set to about $33\,\mathrm{mJ/cm^2}$, which is about 60-fold larger than that of the probe pulses. It was confirmed that the magnetic properties of the pump beam spot remained unchanged by scanning the sample surface after the experiments.

Figure 2(a) shows the experimental results for Case I, by showing the temporal variations of the p-MOKE signal measured at different positions from the center of the pump beam spot, where the distances y from the center are denoted inside each panel. The figure clearly demonstrates that the spinwaves are emitted and propagate from the laser spot. The black solid lines show the best fit with a Gaussian wave packet as given by

$$A \sin(\omega_\mathrm{p} t + \varphi) \exp\left[-\frac{(t - t_\mathrm{p})^2}{2\sigma_\mathrm{t}^2}\right],$$

where A is the amplitude, φ is the phase, t_p is the temporal center, and σ_t is the temporal width of the Gaussian wave packet. The Gaussian profile is employed as the simplest and easiest model[10,12] to determine the center of the wave packet. From the best fit, φ (red) and t_p (blue) are obtained for each curve of different y, as shown in Fig. 2(b). The clear linear dependences enable one to quantify the angular wave number k and the group velocity v_g as $0.55 \pm 0.04\,\mathrm{\mu m^{-1}}$ and 5.2 ± 0.6 km/s, respectively. The phase velocity v_p is then obtained from the relation $v_\mathrm{p} = \omega_\mathrm{p}/k$ as $128 \pm 10\,\mathrm{km/s}$. The average σ_t is estimated to be about $168 \pm 33\,\mathrm{ps}$, which corresponds to the lateral dimension of $21 \pm 6\,\mathrm{\mu m}$ ($= v_\mathrm{p}\sigma_\mathrm{t}$).

Within the context of the spinwave theory, the geometry of Case I allows the generation of the magnetostatic surface wave (MSSW) mode.[18] The dispersion relation of the MSSW mode is given by

$$\omega^2 = \omega_0(\omega_0 + \omega_\mathrm{M}) + \omega_\mathrm{M}^2[1 - \exp(-2kt_\mathrm{f})]/4$$

with two characteristic angular frequencies ω_0 ($= \gamma H_x$) and ω_M ($= \gamma\mu_0 M_\mathrm{S}$), where t_f is the thickness of the ferromagnetic layer, γ is the gyromagnetic ratio, μ_0 is the magnetic permeability, and M_S is the saturation magnetization determined as $(1.17 \pm 0.2) \times 10^6\,\mathrm{A/m}$ by VSM. With the values used in the experiments, the dispersion relation predicts the spinwave angular frequency ω as $(70.1 \pm 0.6) \times 10^9\,\mathrm{rad/s}$, which is relatively close to the experimental value of ω_p. In addition, the MSSW mode is predicted to exhibit a forward phase shift along spinwave propagation. Such a forward phase shift is visualized in Fig. 2(c), where the p-MOKE signal is mapped

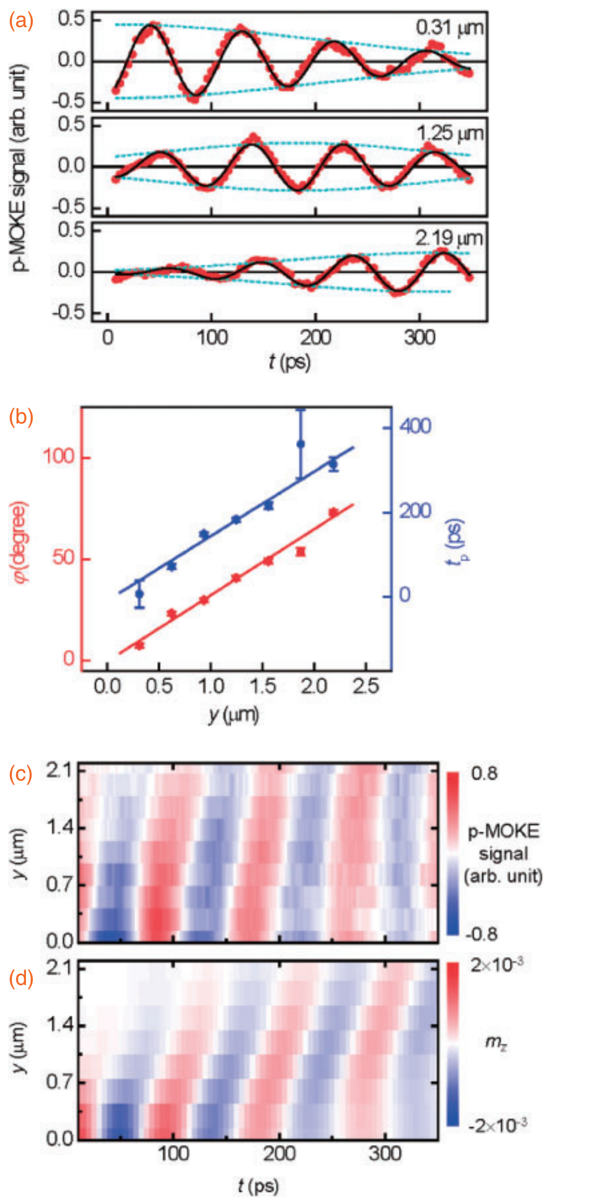

Fig. 2. (a) Temporal variation of the p-MOKE signal for Case I, measured at different positions with the distance y as denoted inside each panel. The black solid lines show the best fit with a Gaussian wave packet, and the cyan solid lines guide the envelope of the wave packet. (b) φ (red) and t_p (blue) with respect to y. The lines show the best linear fit. (c) Two-dimensional map of the experimentally observed spinwaves with respect to the space and time axes. The color inside the maps is proportional to the p-MOKE signal with the scale bar on the right. (d) Simulation results, where the color corresponds to the out-of-plane component m_z of the magnetization unit vector with the scale bar on the right.

onto the space and time coordinates. Figure 2(d) illustrates the micromagnetic prediction[19] of the MSSW mode, where the typical values of the exchange stiffness ($= 1.3 \times 10^{-11}$ J/m), the damping constant ($= 0.01$), and the cell size ($= 5\,\mathrm{nm}$) were used. Here, a two-dimensional array of $1{,}500 \times 1{,}500$ cells under an open boundary condition was used for the calculation. Note that the array size is at least 3 times larger than the experimental scanning range to minimize the finite size effect from the edge. The qualitative agreement with the experimental data verifies the generation of the MSSW mode.

On the other hand, the experimental results for Case II exhibit a distinct behavior, as illustrated in Fig. 3(a). It is

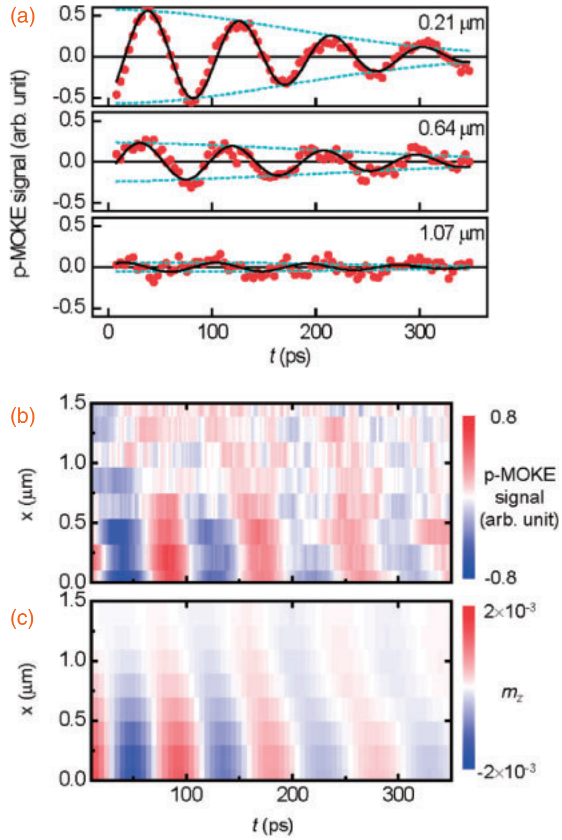

Fig. 3. (a) Temporal variation of the p-MOKE signal for Case II, measured at different positions with the distance x as denoted inside each panel. The black solid lines show the best fit with a Gaussian wave packet, and the cyan solid lines guide the envelope of the wave packet. (b) Two-dimensional map of the experimentally observed spinwaves with respect to the space and time axes. The color inside the maps is proportional to the p-MOKE signal with the scale bar on the right. (c) Simulation results, where the color corresponds to the out-of-plane component m_z of the magnetization unit vector with the scale bar on the right.

seen from the figure that the spinwaves are quickly decayed out within one micrometer. For the geometry of Case II, the magnetostatic backward volume wave (MSBVW) mode is allowed. One of the peculiar features of the MSBVW mode is that it exhibits a backward phase shift with a negative v_p. Such a backward phase shift is visualized by the map shown in Fig. 3(b). From the map, the best estimation of v_p is about -75 ± 20 km/s. Owing to the backward phase shift, the MSBVW mode is hardly emitted outward. Such an observed behavior is again confirmed by micromagnetic simulation, as shown in Fig. 3(c).

In summary, we demonstrate the spinwave emission from the ultrafast demagnetization induced by short laser pulses. Two different spinwave modes of the forward surface (MSSWs) and backward volume (MSBVWs) are observed depending on the relative alignment between the directions of the wavevector and the magnetization. The forward mode propagates over a few micrometers with small dissipation, possibly used for the spinwave experiments.

Acknowledgment This work was supported by the National Research Foundation of Korea (NRF) grant funded by the Ministry of Science, ICT and Future Planning of Korea (MSIP) (2012-003418, 2015R1A2A1A05001698).

1) J. Simon, H. Tanji, S. Ghosh, and V. Vuletic, Nat. Phys. **3**, 765 (2007).
2) A. Khitun, M. Bao, and K. L. Wang, IEEE Trans. Magn. **44**, 2141 (2008).
3) V. V. Kruglyak and R. J. Hicken, J. Magn. Magn. Mater. **306**, 191 (2006).
4) B. Lenk, H. Ulrichs, F. Garbs, and M. Munzenberg, Phys. Rep. **507**, 107 (2011).
5) J. Jorzick, S. O. Demokritov, B. Hillebrands, M. Bailleul, C. Fermon, K. Y. Guslienko, A. N. Slavin, D. V. Berkov, and N. L. Gorn, Phys. Rev. Lett. **88**, 047204 (2002).
6) M. P. Wismayer, B. W. Southern, X. L. Fan, Y. S. Gui, and C. M. Hu, Phys. Rev. B **85**, 064411 (2012).
7) M. Madami, S. Bonetti, G. Consolo, S. Tacchi, G. Carlotti, G. Gubbiotti, F. B. Mancoff, M. A. Yar, and J. Akerman, Nat. Nanotechnol. **6**, 635 (2011).
8) B. Obry, V. I. Vasyuchka, A. V. Chumak, A. A. Serga, and B. Hillebrands, Appl. Phys. Lett. **101**, 192406 (2012).
9) V. Vlaminck and M. Bailleul, Science **322**, 410 (2008).
10) M. Covington, T. M. Crawford, and G. J. Parker, Phys. Rev. Lett. **89**, 237202 (2002).
11) Z. Liu, F. Giesen, X. Zhu, R. D. Sydora, and M. R. Freeman, Phys. Rev. Lett. **98**, 087201 (2007).
12) K. Sekiguchi, K. Yamada, S. M. Seo, K. J. Lee, D. Chiba, K. Kobayashi, and T. Ono, Appl. Phys. Lett. **97**, 022508 (2010).
13) Y. Au, T. Davison, E. Ahmad, P. S. Keatley, R. J. Hicken, and V. V. Kruglyak, Appl. Phys. Lett. **98**, 122506 (2011).
14) K. Sekiguchi, K. Yamada, S. M. Seo, K. J. Lee, D. Chiba, K. Kobayashi, and T. Ono, Phys. Rev. Lett. **108**, 017203 (2012).
15) T. Satoh, Y. Terui, R. Moriya, B. A. Ivanov, K. Adno, E. Saitoh, T. Shimura, and K. Kuroda, Nat. Photonics **6**, 662 (2012).
16) Y. Au, M. Dvornik, T. Davison, E. Ahmad, P. S. Keatley, A. Vansteenkiste, B. Van Waeyenberge, and V. V. Kruglyak, Phys. Rev. Lett. **110**, 097201 (2013).
17) C. Nistor, G. S. D. Beach, and J. L. Erskine, Rev. Sci. Instrum. **77**, 103901 (2006).
18) D. D. Stancil and A. Prabhakar, *Spin Waves: Theory and Applications* (Springer, Heidelberg, 2009) Chap. 5.
19) The "Object Oriented Micromagnetic Framework," developed at NIST, Gaithersburg [http://math.nist.gov/oommf/].